RSC Advances

ROYAL SOCIETY OF CHEMISTRY

www.rsc.org/advances

Table of Contents

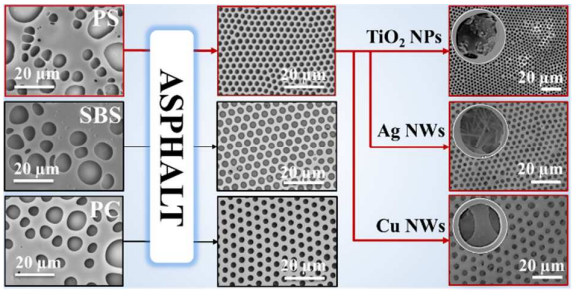

A robust asphalt-assisted breath figure templating approach was explored for general fabrication of porous (hybrid) polymer films with ordered microstructures.

RSC Advances

RSCPublishing

COMMUNICATION

Asphalt-Assisted Assembly of Breath Figures: A Robust Templating Strategy for General Fabrication of Ordered Porous Polymer Films

Cite this: DOI: 10.1039/xoxx00000x

Received ooth December 2014,
Accepted ooth January 2015

DOI: 10.1039/xoxx00000x

www.rsc.org/

Jian-Liang Gong, Bin-Gang Xu* and Xiao-Ming Tao

A robust asphalt-assisted breath figure templating approach has been developed for general fabrication of ordered porous polymer films and functional hybrid films with hierarchical microstructures. The incorporation of desired non-polymeric components, such as titanium dioxide nanoparticles and silver nanowires, shows little influence on the regularity of pore arrays.

Breath figures (BFs) are liquid droplets that can be generated upon exhaling aqueous vapour onto a cold surface.[1,2] Generally, the BF technique is a direct strategy of using self-assembled aqueous droplet arrays as dynamic templates for the fabrication of ordered porous microstructures.[3] This one-step self-assembly approach originated from François et al.[4] is rapid, simple, and most importantly, requires no trivial work on preparing and removing templates because both the condensation and evaporation of water droplets are spontaneous. In the past two decades, the BF-related research has achieved tremendous progress.[3,5-9] Ordered porous microstructures with a size varying from 200 nm to 20 μm have been directly constructed from a variety of film-forming materials including series of polymers with different architectures,[10-14] hybrids of polymer and inorganic components,[15, 16] carbon nanomaterials,[17,18] supramolecular polymers,[19] and even inorganic nanoparticles,[20,21] for more and more promising applications, such as microfabrication, microreactors, biosensors, cell culture, selective separation, functional and responsive surfaces.[6,7]

Although a vast variety of film-forming materials have been exploited by BF technique, it is still difficult to find a more universal strategy to prepare ordered porous microstructures. This is because different film-forming materials often require different BF conditions, which makes the process more empirical. In addition, due to the non-isothermal and non-equilibrium character of BF, subtle changes during the process often lead to the formation of disorder microstructures.[7,8] This inevitably results in the poor reproducibility of ordered microstructures when replacing the substrates or introducing desired functional components is required. Therefore, for most of the reported film-forming materials, repeatedly laborious efforts have to be made on exploring the optimal BF conditions to obtain controllable microstructures, such as modification of target materials, adjusting solution concentration, humidity and temperature.[3,6,8] In this communication, we present a robust and universal BF templating strategy for the formation of ordered porous microstructures by exploring an efficient oligomer additive. The addition of asphalt can effectively assist the target materials to form microporous films with greatly promoted regularity on selectable substrates in a wide concentration range of casting solution.

A typical BF process is usually performed by casting a certain volume of polymer solution on a substrate under nonsolvent vapor. The employed nonsolvent vapour is often generated by a moist airflow, and the chosen solvents for dissolving polymers generally have a low-boiling point and are immiscible with water. To exemplify the feasibility of asphalt-assisted BF technique, here we firstly chose a nonpolar linear polystyrene (PS) as the film-forming material because its block copolymers and modified analogues are the most widely used polymer types by BF technique, but PS itself does not form well-ordered pore arrays under most conditions.[3] The number-average molecular weight (M_n) of PS and asphalt determined by gel permeation chromatography (GPC) was 129,600 and 1,000, respectively. Asphalt is a mixture of oligomers, mainly comprising four different components including saturated hydrocarbons, naphthene aromatics, polar aromatics, and asphaltenes. These components, particularly polar aromatics and naphthene aromatics, have similar solubility values with PS.[22] This enables asphalt good miscibility with PS.

PS/asphalt (PSA) solutions were prepared by dissolving PS and asphalt in carbon disulphide (CS_2) according to a certain weight ration. To minimize the uncertainties caused by flow disturbing, the BF process was modified by casting the prepared solution on a desired substrate in a sealed cell saturated with aqueous vapour at room temperature (about 25 ^oC). When the clear liquid film became an opaque and solid film with the evaporation of solvent, it was taken out for vacuum drying to complete removal of residual solvent and water. And then a gold layer of about 2 nm thickness was sputter-coated on the film surface for scanning electronic microscopy (SEM) observation. As shown in Fig. 1, the morphology evolution of films

on glass substrates cast from 25 mg mL^{-1} PSA solutions was clearly observed with the increasing asphalt contents. Without the assistance of asphalt, only irregular pores with largely different size were observed in PS films (Fig. 1a). While after introducing 10 wt% asphalt, the pore size was decreased obviously and became relatively homogeneous (Fig. 1b). And increasing asphalt content was conducive to form more uniform pores, as shown in Fig. 1c. When the content was increased to 30 wt%, uniform round pores were found in local film regions, coexisting with irregular pores (Fig. 1d). Slightly increasing the asphalt fraction to 35 wt%, ordered arrays with round pores, namely the typical honeycomb porous microstructures, were observed as expected in large scale (Fig. 1e). The continuing increase of asphalt could further enhance the regularity of pore arrays, as demonstrated in Fig. 1f. And the similar highly ordered microstructures illustrated that enlarging the fraction of asphalt to 50 wt% has no influence on the regularity of pore arrays (Fig. 1g). Even when the asphalt content exceeded PS, highly regular honeycomb porous arrays still could be obtained (Fig. 1h). Only the average pore size was decreased from 4.42 μm (35 wt% asphalt) to 3.02 μm (60 wt% asphalt). Nevertheless, further raising the asphalt proportion would result in the formation of less regular honeycomb microstructures. As shown in Fig. 1i, some distorted pores were found to intersperse in the pore arrays after 5% more asphalt was added. And a mottled surface involving the deformed pores and non-porous areas was obtained when the added asphalt was over 80 wt% (Fig. 1j). This is probably because rigid PS component is plasticized and softened seriously by semi-solid asphalt, which thus cannot effectively maintain the formed microstructures. Only few isolated pores were irregularly distributed in non-porous areas when asphalt content was up to 90%. In some partial film areas, the imprint of water droplets could be observed (Fig. 1k), which clearly indicates that over addition of asphalt will result in the collapse of microstructures. And this can be further demonstrated by casting asphalt/CS_2 solution on a glass substrate using the BF method, because only buckling features were observed in the asphalt film rather than porous structures, as demonstrated in Fig. 1l. The morphology evolution of PSA films above suggests that asphalt can efficiently assist PS solution to form ordered porous microstructures in a wide additive range (from 35 wt% to 60 wt%).

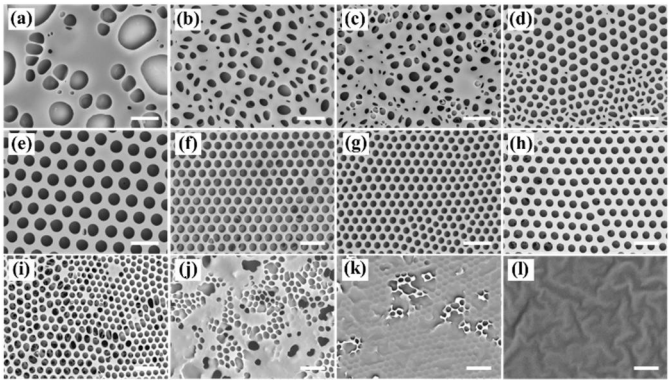

Fig. 1 SEM images of morphological evolution of PSA films on glass substrates with increasing asphalt contents: (a) 0, (b) 10 wt%, (c) 20 wt%, (d) 30 wt%, (e) 35 wt%, (f) 40 wt%, (g) 50 wt%, (h) 60 wt%, (i) 65 wt%, (j) 80 wt%, (k) 90 wt%, and (l) 100 wt%. The concentration of all casting solutions was fixed at 25 mg mL^{-1}. The scale bars are 10 μm.

The influence of solution concentration on the polymer film morphology was further investigated by fixing the weight ratio of PS to asphalt at 1. As shown in Fig. 2a-d, the typical morphologies of films prepared from PSA solutions all possess a highly ordered hexagonal pore arrays regardless of the solution concentration ranging from 10 mg mL^{-1} to 50 mg mL^{-1}. Graphical histograms visually reflect that the pore size distribution of each PSA film sample is narrow, indicating the formation of uniform pores. While without the addition of asphalt, neat PS films cast from a wide solution concentration displayed a disordered porous microstructure with a broad size distribution (Fig. 2e, g and h). Only the pore size of films cast at 20 mg mL^{-1} was relatively homogeneous (Fig. 2f). This means that the addition of asphalt contributes to the formation of ordered porous films by extending the workable concentration of casting solution from 10 mg ml^{-1} to 50 mg ml^{-1}. The dependence of pore size on the concentration of PSA and PS solution was further plotted in Fig. 2i and j, respectively. The average pore sizes of PSA films with a standard deviation were 1.93 μm (0.12) at 10 mg mL^{-1}, 4.11 μm (0.17) at 20 mg mL^{-1}, 3.89 μm (0.19) at 30 mg mL^{-1}, and 2.86 μm (0.12) at 50 mg mL^{-1}, showing a decreasing trend with the increased concentration of solution after 10 mg mL^{-1}. Basically, the average size of porous PS films also presents a decrease by increasing solution concentration. Correspondingly at the same concentrations of 10 mg mL^{-1}, 20 mg mL^{-1} and 30 mg mL^{-1}, the average sizes of porous PS films were 8.50 μm, 6.89 μm, and 5.43 μm, but their standard deviations were up to 5.22, 0.68, and 0.47, respectively. Especially at 50 mg mL^{-1}, the resulted PS films even roughly appeared a bimodal size distribution because of the coexistence of small satellite pores (2.41 μm, 0.93) and large main pores (12.00 μm, 8.07). These results clearly indicate that, in a similar BF condition, the introduction of asphalt can effectively reduce the pore size and greatly narrow the size distribution of polymer films.

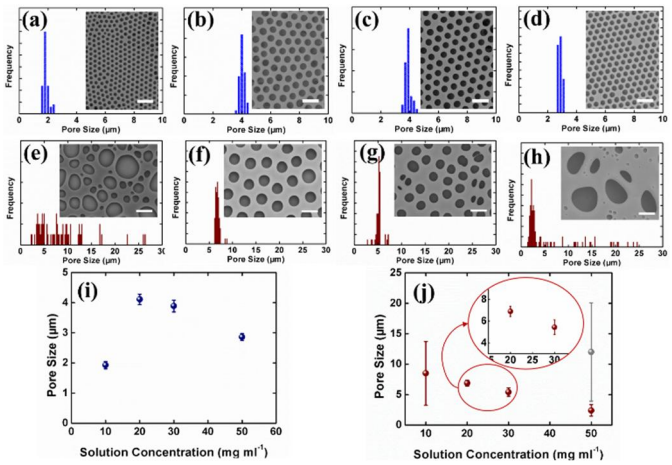

Fig. 2 Typical SEM images and pore size distribution of PSA (a-d) and PS (e-h) films cast from different solution concentrations: (a) and (e) 10 mg mL^{-1}, (b) and (f) 20 mg mL^{-1}, (c) and (g) 30 mg mL^{-1}, (d) and (h) 50 mg mL^{-1}. Plot of the dependence of pore size on the concentration of (i) PSA solution and (j) PS solution. The introduced weight amount of asphalt in PSA films is equal to PS. The pore size was measured along the major axis of pores and grouped by every 0.2 μm in histograms. The scale bars are 10 μm.

Besides assisting polymer solution at a non-optimal concentration to form highly regular microstructures in a broader concentration range, asphalt-assisted BF technique also shows good robustness on changing substrates or incorporating functional nanocomponents, which could meet more actual requirements. As shown in Fig. 3a and b, ordered porous films were facilely obtained when the glass substrate was replaced by copper (Cu) foil and silicon wafer, respectively. Even PSA solution was directly cast on water surface, typical honeycomb porous features can also be observed (Fig. 3c). When different nonplanar substrates were used, such as transmission

electron microscope (TEM) grids, ordered porous APS films can act a coating to effectively contour the whole object regardless of the surface pattern and size. SEM images (Fig. 3d-f and insets) reveal that honeycomb pore arrays exist around the surface profile of objects, giving rise to a multilevel surface morphology. Loading a desired inorganic component into porous polymeric supporter is an effective approach of ensuring its maximum performance. Maintaining the porous microstructures without collapse is the key of fabricating such functional organic/inorganic hybrid materials. As shown in Fig. 3g-i, PSA films incorporated 10 wt% titanium dioxide nanoparticles (TiO_2 NPs), 5 wt% silver nanowires (Ag NWs), and 3% Cu nanowires (Cu NWs) were revealed by SEM, respectively. The similar highly regular honeycomb patterns with APS films illustrate that the incorporated nanocomponents have little influence on the regularity of pore arrays. Through the pore holes, some nanocomponents, such as TiO_2 NPs and Ag NWs, were clearly observed from a close view (insets of Figure 3g-i). Ti, Ag, and Cu elements determined by energy dispersive X-ray spectrometer (EDX) further confirm the successful incorporation of designated nanocomponents (Figure 3j-l). These results indicate the successful preparation of hybrid films with a hierarchical microstructure, which combines the merits of polymer micropores and functional nanocomponents.

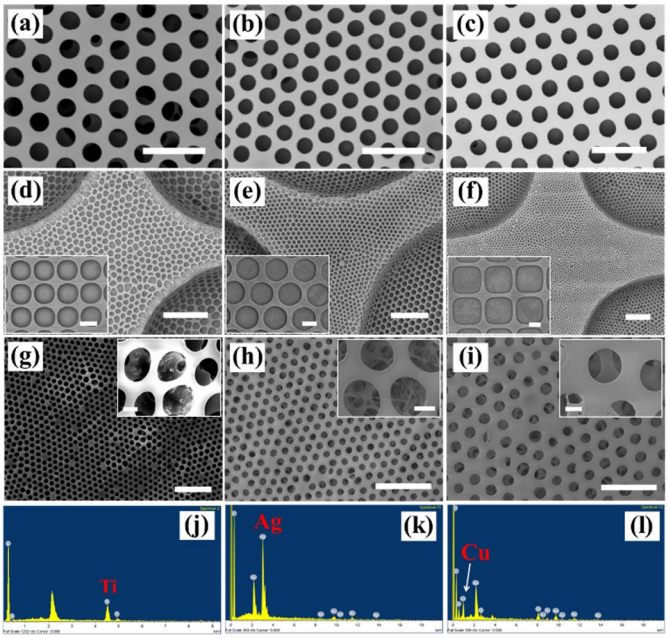

Fig. 3 SEM images of PSA films (PS/asphalt=1/1, w/w) on different substrates including planar substrates: (a) copper foil, (b) silicon wafer, (c) water surface, and nonplanar surface constructed by placing different copper grids on planar substrates: (d) 200 mesh TEM grid with square pattern, (e) 150 mesh TEM grid with hexagonal pattern, (f) 100 mesh TEM grid with square pattern. The insets in (d)-(f) were SEM images at low magnifications. SEM images and EDX spectrums of PSA films incorporated with (g) and (j) 10 wt% TiO_2 NPs, (h) and (k) 5 wt% Ag NWs, and (i) and (l)3 wt% Cu NWs. The insets in (g)-(i) are close view of pores. Scale bars: (a)-(c) 10 μm; (d)-(f) 20 μm and 100 μm (insets); (g)-(i) 20 μm and 2 μm (insets).

Three other common polymers including a thermoplastic PS-*b*-polybutadiene-*b*-PS (SBS, M_n=113,800), an engineering plastic polycarbonate (PC, M_n=26,500), and a biodegradable polymer poly(ethylene oxide) (PEO, M_n=500,000) were used to verify the universality of this strategy of assisting targeted materials to form more regular porous microstructures. They were dissolved in CS_2 or chloroform ($CHCl_3$), and cast on glass substrates by the BF technique, respectively. The irregular patterns revealed by optical microscopy (OM) indicate that both SBS/CS_2 and PC/$CHCl_3$ solutions at 12.5 mg mL^{-1} were not suitable for the formation of ordered porous films (Fig. 4a and b). While after the addition of small asphalt, the pore size became more homogeneous obviously. And ordered porous films with uniform size were obtained when about 30 wt% and 35 wt% asphalt were introduced into the SBS films (Fig. 4d) and PC films (Fig. 4e), respectively. PEO generally shows a semicrystalline nature. Nonporous microstructures were found when its $CHCl_3$ solution was cast under aqueous vapour (Fig. 4c). Instead, large spherulites tightly interconnected with each other were clearly observed by polarizing OM (POM, insets of Fig. 4c). Even for this water-soluble semi-crystalline polymers, porous microstructures with relatively uniform size were observed by OM when 50 wt% asphalt was introduced (Fig. 4f). And POM shows that the size of PEO spherulites was reduced drastically, which are space-filling even in the PEO/asphalt film (insets of Fig. 4f).

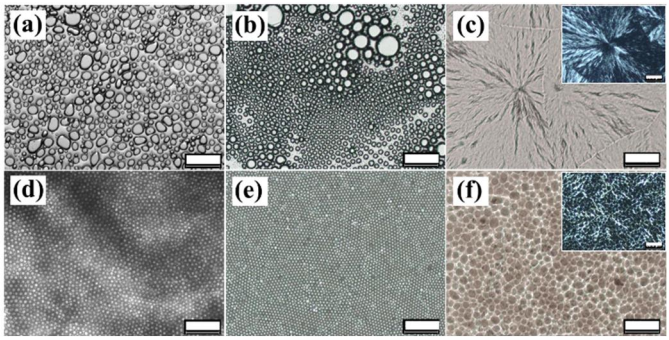

Fig. 4 Optical micrographs of polymer films without asphalt cast from 12.5 mg ml^{-1} (a) SBS/CS_2, (b) PC/$CHCl_3$, and (c) PEO/$CHCl_3$ solutions. Optical micrographs (d) SBS/asphalt, (e) PC/asphalt, and (f) PEO/asphalt films after introducing 30 wt%, 35 wt%, and 50 wt% asphalt. The insets are polarized optical micrographs. The scale bars are 50 μm.

Conclusions

We have demonstrated a robust modified BF approach assisted by asphalt to fabricate ordered porous polymer films in a more flexible conditions. By adjusting the addition of asphalt at an appropriate range, PS solutions at non-workable concentrations were successfully used to obtain regular porous microstructures. The formation of ordered porous films was also exemplified on various substrates with different surface energy, including rough surfaces. And further introduction of functional nanocomponents also shows little influence on the regularity of film pore arrays. This easily approachable strategy was also generally suitable for other polymers, such as SBS, PC and PEO, to prepare porous films with greatly promoted regularity. The formation mechanism of asphalt-assisted BF process is currently under investigation, and the promising applications of polymer/asphalt films such as photo-catalysis will be explored in our future work.

Acknowledgements

The authors acknowledge The Hong Kong Polytechnic University for funding supports of this work. Gong Jianliang would also like to thank The Hong Kong Polytechnic University for providing him with a postgraduate scholarship.

Notes and references

Nanotechnology Centre, Institute of Textiles and Clothing, The Hong Kong Polytechnic University, Hung Hom, Kowloon, Hong Kong, P. R. China
*To whom correspondence should be addressed.
E-mail: tcxubg@polyu.edu.hk; Tel: +852-2766 4544

1 L. Rayleigh, *Nature*, 1912, **90**, 436-438.
2 L. Rayleigh, *Nature*, 1911, **86**, 416-417.
3 U. H. F. Bunz, *Adv. Mater.*, 2006, **18**, 973-989.
4 G. Widawski, M. Rawiso and B. François, *Nature*, 1994, **369**, 387-389.
5 A. Muñoz-Bonilla, M. Fernández-García and J. Rodriguez-Hernandez, *Prog. Polym. Sci.*, 2014, **39**, 510-554.
6 L. S. Wan, L. W. Zhu, Y. Ou and Z. K. Xu, *Chem. Commun.*, 2014, **50**, 4024-4039.
7 H. Bai, C. Du, A. Zhang and L. Li, *Angew. Chem., Int. Ed.*, 2013, **52**, 12240-12255.
8 M. Hernández-Guerrero and M. H. Stenzel, *Polym. Chem.,* 2012, **3**, 563-577.
9 P. Escalé, L. Rubatat, L. Billon and M. Save, *Eur. Polym. J.*, 2012, **48**, 1001-1025.
10 W. Wang, C. Du, X. Wang, X. He, J. Lin, L. Li and S. Lin. *Angew. Chem.*, *Int. Ed.*, 2014, **53**, 12116-12119.
11 Z. Li, X. Ma, D. Zang, B. Shang, X. Qiang, Q. Hong and X. Guan, *RSC Adv.*, 2014, **4**, 49655-49662.
12 L. Li, Y. Zhong, J. Gong, J. Li, C. Chen, B. Zeng and Z. Ma, *Soft Matter*, 2011, **7**, 546-552.
13 J. Gong, B. Xu, X. Tao and L. Li, *Plasma Process. Polym.*, 2014, **11**, 1001-1009.
14 H. Ma, P. Gao, Y. Zhang, D. Fan, G. Li, B. Du and Q. Wei, *RSC Adv.*, 2013, **3**, 25291-25295.
15 J. Gong, L. Sun, Y. Zhong, C. Ma, L. Li, S. Xie and V. Svrcek, *Nanoscale*, 2012, **4**, 278-283.
16 C. Y. Ma, Y. W. Zhong, J. Li, C. K. Chen, J. L. Gong, S. Y. Xie, L. Li and Z. Ma, *Chem. Mater.*, 2010, **22**, 2367-2374.
17 S. H. Lee, H. W. Kim, J. O. Hwang, W. J. Lee, J. Kwon, C. W. Bielawski, S. R. Rodney and S. O. Kim, *Angew. Chem.*, *Int. Ed.,* 2010, **122**, 10282-10286.
18 S. H. Lee, J. S. Park, B. K. Lim, C. B. Mo, W. J. Lee, J. M. Lee, S. H. Hong and S. O. Kim, *Soft Matter*, 2009, **5**, 2343-2346.
19 J. Chen, X. Yan, Q. Zhao, L. Li and F. Huang, *Polym. Chem.*, 2012, **3**, 458-462.
20 Y. Saito, M. Shimomura and H. Yabu, *Chem. Commun.*, 2013, **49**, 6081-6083.
21 Y. Saito, M. Shimomura and H. Yabu, *Macromol. Rapid Commun*., 2014, 20, 1763-1769.
22 R. M. Ho, A. Adedeji, D. W. Giles, D. A. Hajduk, C. W. Macosko and F. S. Bates, *J. Polym. Sci. Pt. B-Polym. Phys.*, 1997, **35**, 2857-2877.

